

## Control of Electronic Structure of Graphene by Various Dopants and Their Effects on a Nanogenerator

Hyeon-Jin Shin,<sup>†,‡</sup> Won Mook Choi,<sup>†</sup> Dukhyun Choi,<sup>†,§</sup> Gang Hee Han,<sup>‡</sup>  
Seon-Mi Yoon,<sup>†</sup> Hyun-Kyu Park,<sup>||</sup> Sang-Woo Kim,<sup>||</sup> Yong Wan Jin,<sup>†</sup> Sang Yoon Lee,<sup>†</sup>  
Jong Min Kim,<sup>⊥</sup> Jae-Young Choi,<sup>\*,†</sup> and Young Hee Lee<sup>\*,‡</sup>

*Display Lab, Samsung Advanced Institute of Technology, Yongin 446-712, South Korea; BK21 Physics Division, Department of Energy Science, and Center for Nanotubes and Nanostructured Composites, Sungkyunkwan Advanced Institute of Nanotechnology, Sungkyunkwan University, Suwon 440-746, South Korea; School of Advanced Materials Science and Engineering, Sungkyunkwan Advanced Institute of Nanotechnology, Center for Human Interface Nanotechnology, Sungkyunkwan University, Suwon 440-746, South Korea; and Frontier Research Lab, Samsung Advanced Institute of Technology, Yongin 446-712, South Korea*

Received June 12, 2010; E-mail: jaeyoung88.choi@saumsung.com; leeyoung@skku.edu

**Abstract:** It is essential to control the electronic structure of graphene in order to apply graphene films for use in electrodes. We have introduced chemical dopants that modulate the electronic properties of few-layer graphene films synthesized by chemical vapor deposition. The work function, sheet carrier density, mobility, and sheet resistance of these films were systematically modulated by the reduction potential values of dopants. We further demonstrated that the power generation of a nanogenerator was strongly influenced by the choice of a graphene electrode with a modified work function. The off-current was well quenched in graphene films with high work functions (Au-doped) due to the formation of high Schottky barrier heights, whereas leakage current was observed in graphene films with low work functions (viologen-doped), due to nearly ohmic contact.

### 1. Introduction

The electronic properties of graphene sheets have recently attracted much experimental and theoretical research interest. A single graphene layer is a semimetal or zero-gap semiconductor, and has excellent electronic properties, such as high mobility ( $200\,000\text{ cm}^2\text{ V}^{-1}\text{ s}^{-1}$ ), room-temperature quantum Hall effect, and high mechanical elasticity (elastic modulus of about 1 TPa).<sup>1–6</sup> In addition, high flexibility, optical transmittance, and chemical stability are other technological advantages of single

graphene layers.<sup>7–9</sup> These superb characteristics open new potential applications of graphene in flexible and transparent electronic devices.<sup>10–13</sup>

The work function is an important factor governing the application of graphene as an electrode, for instance, in solar cells and light emitting diodes. The work function determines the band alignment in the contact to facilitate selective electron and hole transport.<sup>14,15</sup> The work functions of monolayer and bilayer graphenes were measured in a previous study, and were further tuned by the implementation of an electric field.<sup>16</sup> Changes in the work function of monolayer graphene ranged from 4.5 eV for pristine graphene under ambient and dry nitrogen conditions to 4.8 eV under an electric field. Although this result implies that the work function of graphene can easily

<sup>†</sup> Display Lab, Samsung Advanced Institute of Technology.

<sup>§</sup> Present Address: Department of Mechanical Engineering, School of Engineering, Kyung Hee University, Yongin 449-701, South Korea.

<sup>‡</sup> BK21 Physics Division, Department of Energy Science, and Center for Nanotubes and Nanostructured Composites, Sungkyunkwan Advanced Institute of Nanotechnology, Sungkyunkwan University.

<sup>||</sup> School of Advanced Materials Science and Engineering, Sungkyunkwan Advanced Institute of Nanotechnology, Center for Human Interface Nanotechnology, Sungkyunkwan University.

<sup>⊥</sup> Frontier Research Lab, Samsung Advanced Institute of Technology.

- (1) Novoselov, K. S.; Geim, A. K.; Morozov, S. V.; Jiang, D.; Zhang, Y.; Dubonos, S. V.; Grigorieva, I. V.; Firsov, A. A. *Science* **2004**, *306*, 666–669.
- (2) Geim, A. K.; Novoselov, K. S. *Nat. Mater.* **2007**, *6*, 183–191.
- (3) Zhang, Y.; Tan, Y.-W.; Stormer, H. L.; Kim, P. *Nature* **2005**, *438*, 201–204.
- (4) Luk'yanchuk, I. A.; Kopelevich, Y. *Phys. Rev. Lett.* **2004**, *93*, 166402–166406.
- (5) Novoselov, K. S.; Jiang, Z.; Zhang, Y.; Morozov, S. V.; Stormer, H. L.; Zeitler, U.; Maam, J. C.; Boebinger, G. S.; Kim, P.; Geim, A. K. *Science* **2007**, *315*, 1379.
- (6) Bolotin, K. I.; Sikes, K. J.; Jiang, Z.; Fundenberg, G.; Hone, J.; Kim, P.; Stormer, H. L. *Solid State Commun.* **2008**, *146*, 351–355.

(7) Wallace, P. R. *Phys. Rev.* **1947**, *71*, 622–634.

(8) Chen, J.-H.; Jang, C.; Xiao, S.; Ishigami, M.; Fuhrer, M. S. *Nat. Nanotechnol.* **2008**, *3*, 206–209.

(9) Lee, C.; Wei, X.; Kysar, J. W.; Hone, J. *Science* **2008**, *321*, 385–388.

(10) Blake, P.; Brimicombe, P. D.; Nair, R. R.; Booth, T. J.; Jiang, D.; Schedin, F.; Ponomarenko, L. A.; Morozov, S. V.; Gleason, H. F.; Hill, E. W.; Geim, A. K.; Novoselov, K. S. *Nano Lett.* **2008**, *8*, 1704–1708.

(11) Wang, X.; Zhi, L.; Müllen, K. *Nano Lett.* **2008**, *8*, 323–327.

(12) Güneş, F.; Han, G. H.; Kim, K. K.; Kim, E. S.; Chae, S. J.; Park, M. H.; Jeong, H.-K.; Lim, S. C.; Lee, Y. H. *NANO* **2009**, *4*, 83–90.

(13) Wu, J.; Agrawal, M.; Becerril, H. A.; Bao, Z.; Liu, Z.; Chen, Y.; Peumans, P. *ACS Nano* **2010**, *4*, 43–48.

(14) Ishii, H.; Sugiyama, K.; Ito, E.; Seki, K. *Adv. Mater.* **1999**, *11*, 605–625.

(15) Jiang, J.; Krauss, T. D.; Brus, L. E. *J. Phys. Chem. B.* **2000**, *104*, 11936–11941.

(16) Yu, Y.-J.; Zhao, Y.; Ryu, S.; Brus, L. E.; Kim, K. S.; Kim, P. *Nano Lett.* **2009**, *9*, 3430–3434.

be tuned, this approach is still limited for use in electroactive devices. A robust approach to controlling the work function must be demonstrated in order to make single-layer graphene suitable for use in a number of applications.

AuCl<sub>3</sub> dopant provides p-type doping in carbon nanotubes, as observed by optical absorption spectroscopy and Raman spectroscopy.<sup>17</sup> In contrast, viologen and  $\beta$ -nicotinamide adenine dinucleotide, reduced dipotassium salt (NADH) generate n-type doping in carbon nanotube transistors.<sup>18,19</sup> Although the type conversion of semiconducting carbon nanotubes using such dopants may be accomplished by simple charge transfer based on a reduction potential argument, the correlations among modified work function, sheet carrier density, mobility, and sheet resistance are not clearly understood.<sup>20–25</sup> The doping of graphene may also behave differently due to the metallic linear dispersion relationship of graphene near the Dirac point, as well as its two-dimensionality.

The purpose of this study is 2-fold: (i) to determine a chemical approach to modulate the electronic structure of few-layer graphene, and (ii) to demonstrate the effects of this approach in a realistic nanogenerator model. The work function of few-layer graphene synthesized by chemical vapor deposition (CVD) was maintained between 4.0 and 4.8 eV by chemical dopants with various reduction potentials. By using a work function controlled graphene sheet as a top cathode electrode in a nanogenerator, we demonstrate that energy scavenging performance can be modulated based on the Schottky barrier model.

## 2. Experimental Section

**2.1. Graphene Film Preparation.** Graphene films were synthesized on Ni thin film (300 nm)/SiO<sub>2</sub> (300 nm)/Si substrate by rapid thermal chemical vapor deposition (RT-CVD).<sup>12,26</sup> The temperature was increased from room temperature to 1000 °C in 5 min. An initial reduction of the Ni substrate was carried out in a hydrogen gas flow of 45 sccm for 30 min at 1000 °C. Graphene was synthesized at 1000 °C by a gas flow of H<sub>2</sub>/C<sub>2</sub>H<sub>2</sub>: 2/45 sccm, and the chamber was then cooled down to room temperature under the same atmosphere at a cooling rate of 160 °C min<sup>-1</sup>. Graphene layers ranging from monolayer to 30 layers were obtained by controlling the growth time. Cu foil was also used to synthesize monolayer graphene to check the layer dependence on doping. The synthesis method has been described elsewhere.<sup>27,28</sup>

After synthesis, poly (methyl methacrylate)(PMMA) was coated onto the synthesized graphene films, followed by dipping into

etchant (HNO<sub>3</sub>) solution. When the catalyst film (Ni or Cu) was completely etched away, the resulting graphene sheets coated with PMMA were rinsed in deionized water several times to wash away any etchant residues. Then, the PMMA-coated graphene sheets were transferred onto polyethylene terephthalate (PET) substrate. PMMA was removed by acetone after the graphene had completely adhered onto the PET substrate.

### 2.2. Doped Graphene Film Preparation and Characterization.

Gold chloride (AuCl<sub>3</sub>) powder, 2,3-dichloro-5,6-dicyanobenzoquinone (DDQ), and 1,1'-dibenzyl-4,4'-bipyridinium dichloride (BV<sup>2+</sup>) for use as a dopant were purchased from Sigma-Aldrich. AuCl<sub>3</sub> and DDQ powder were dissolved in nitromethane to yield 10 mM of solution each. BV<sup>0</sup> solution (10 mM) was prepared by BV<sup>2+</sup> reduction in a biphasic solution of water/toluene as described in previous work.<sup>18</sup> To control the work function of graphene, the dopant solution was dropped onto the graphene film and spin-coated at 2000 rpm for 1 min after 30 s residual time.

The sheet carrier density, mobility, and sheet resistance of graphene were measured by the van der Pauw method using a Hall measurement (ACCENT semiconductor UK/HL 5500PC) at room temperature, 0.3 T. Raman spectroscopy (Renishaw, RM-1000 Invia) with an excitation energy of 2.41 eV (514 nm, Ar<sup>+</sup> ion laser) was used to characterize the optical properties of graphene films on SiO<sub>2</sub>/Si substrates. The work functions of the tailored graphene sheets were measured by UV photoelectron spectroscopy (UPS; Gammadata VUV 5050) using a He II discharge lamp ( $h\nu = 40.8$  eV). The work function was determined using the secondary-electron cutoff of the UPS using gold as a reference. The position of the Fermi level was calibrated by measuring the Fermi edge of gold. The doped graphene structure was characterized using a scanning tunneling microscope (SEM: JEOL JSM 6500).

**2.3. Nanogenerator Fabrication and Evaluation.** ZnO nanorods were synthesized using an aqueous-solution method on indium tin oxide (ITO)-coated polyethersulfone (PES) substrate with an ITO thickness of 350 nm and sheet resistance of  $\sim 30 \Omega/\text{sq}$ . Zinc acetate solution (Zn(CH<sub>3</sub>COO)<sub>2</sub>·2H<sub>2</sub>O, 0.01 M in ethanol) was used as a seed material to synthesize high-quality ZnO nanorods. The seed solution was dropped onto the substrate and spin-coated at 1000 rpm for 60 s, and then baked on a hot plate at 100 °C for 10 min. ZnO nanorods were formed in aqueous solution including zinc nitrate hexahydrate (Zn(NO<sub>3</sub>)<sub>2</sub>·6H<sub>2</sub>O, 0.025 M), hexamethylenetetramine (0.025 M), and deionized water (250 mL). The main growth of ZnO nanorods took place at 95 °C for 3 h.

Current–voltage measurements to evaluate the formation of Schottky-contact between ZnO-nanorod arrays and a graphene top electrode were carried out using an Agilent 4156A parameter analyzer. A Keithley 6485 Picoammeter was used for low-noise current measurements in order to detect currents generated by the piezoelectric nanodevices.

## 3. Results and Discussion

**3.1. Electronic Structure Tuning Using Dopants with Different Reduction Potential.** Figure 1 is an electron transfer mechanism between graphene and dopant. The material parameters of dopants with various reduction potential values are listed in Table 1. The reduction potential is exclusively correlated with the doping concentration of graphene. Au<sup>3+</sup> and DDQ have positive reduction potentials (or negative Gibbs free energy obtained from the Nernst equation).<sup>29,30</sup> The larger reduction

- (17) Kim, K. K.; Bae, J. J.; Park, H. K.; Kim, S. M.; Geng, H.-Z.; Park, K. A.; Shin, H.-J.; Yoon, S.-M.; Benayad, A.; Choi, J.-Y.; Lee, Y. H. *J. Am. Chem. Soc.* **2008**, *130*, 12757–12761.
- (18) Kim, S. M.; Jang, J. H.; Kim, K. K.; Park, H. K.; Bae, J. J.; Yu, W. J.; Lee, I. H.; Kim, G.; Loc, D. D.; Kim, U. J.; Lee, E.-H.; Shin, H.-J.; Choi, J.-Y.; Lee, Y. H. *J. Am. Chem. Soc.* **2009**, *131*, 327–331.
- (19) Kang, B. R.; Yu, W. J.; Kim, K. K.; Park, H. K.; Kim, S. M.; Park, Y.; Kim, G.; Shin, H.-J.; Kim, U. J.; Lee, E.-H.; Choi, J.-Y.; Lee, Y. H. *Adv. Funct. Mater.* **2009**, *19*, 2553–2559.
- (20) Nomura, K.; MacDonald, A. H. *Phys. Rev. Lett.* **2006**, *96*, 256602.
- (21) Ando, T. *J. Phys. Soc. Jpn.* **2006**, *75*, 074716.
- (22) Schedin, F.; Geim, A. K.; Morozov, S. V.; Hill, E. W.; Blake, P.; Katsnelson, M. I.; Novoselov, K. S. *Nat. Mater.* **2007**, *6*, 652–655.
- (23) Chen, J.-H.; Jang, C.; Adam, S.; Fuhrer, M. S.; Williams, E. D. *Nat. Phys.* **2008**, *4*, 377–381.
- (24) Ponomarenko, L. A.; Yang, R.; Mohiuddin, T. M.; Katsnelson, M. I.; Novoselov, K. S.; Morozov, S. V.; Zhukov, A. A.; Schedin, F.; Hill, E. W.; Geim, A. K. *Phys. Rev. Lett.* **2009**, *102*, 206603.
- (25) Chen, J.-H.; Cullen, W. G.; Jang, C.; Fuhrer, M. S.; Williams, E. D. *Phys. Rev. Lett.* **2009**, *102*, 236805.
- (26) Chae, S. J.; Güneş, F.; Kim, K. K.; Kim, E. S.; Han, G. H.; Kim, S. M.; Shin, H.-J.; Yoon, S.-M.; Choi, J.-Y.; Park, M. H.; Yang, C. W.; Pribat, D.; Lee, Y. H. *Adv. Mater.* **2009**, *21*, 2328–2333.

- (27) Li, X.; Cai, W.; An, J.; Kim, S.; Nah, J.; Yang, D.; Piner, R.; Velamakanni, A.; Jung, I.; Tutuc, E.; Banerjee, S. K.; Colombo, L.; Ruoff, R. S. *Science* **2009**, *324*, 1312–1314.
- (28) Güneş, F.; Shin, H.-J.; Biswas, C.; Han, G. H.; Kim, E. S.; Chae, S. J.; Choi, J.-Y.; Lee, Y. H. *ACS nano* **2010**, *4*, 4595–4600.
- (29) Kong, B.-S.; Geng, J.; Jung, H.-T. *Chem. Commun.* **2009**, 2174–2176.
- (30) Ciprelli, J.-L.; Clarisse, C.; Delabouglise, D. *Synth. Met.* **1995**, *74*, 217.

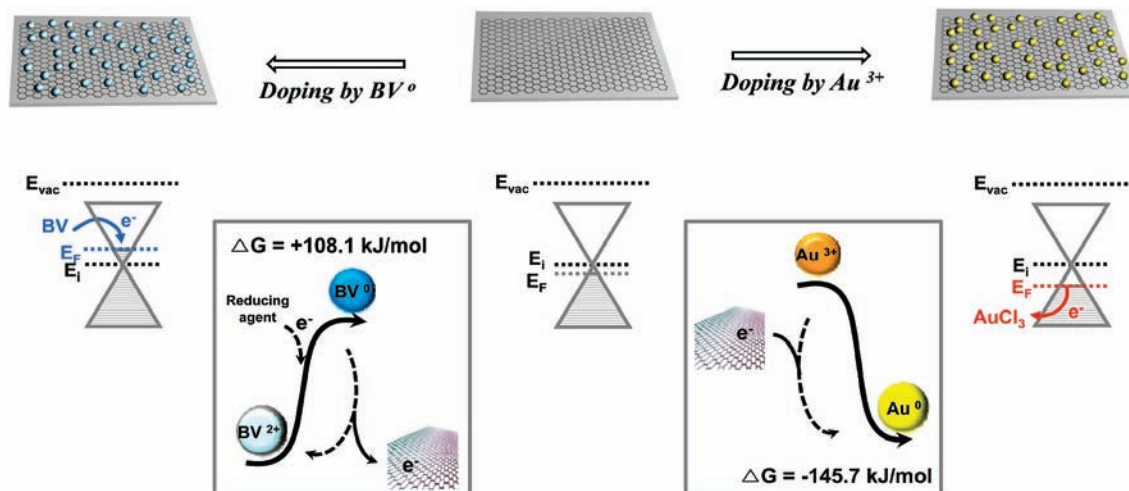
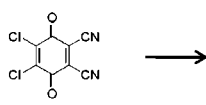
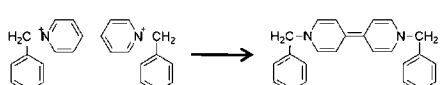


Figure 1. Modulation of electronic structure by differences of reduction potentials.

Table 1. Material Parameters of Various Dopants: Nomenclature, Structure, Reduction Potential, and Gibbs Free Energy

Material	Structure	Reduction potential (vs SHE) $E^{\circ}$ (V)	Gibbs free energy $\Delta G$ (kJ/mol)	Relative Gibbs energy (vs Graphene)
Gold chloride (III)	$Au^{3+} \longrightarrow Au^0$	1.51 <sup>29</sup>	-145.7	Spontaneous ( $\Delta G < 0$ )
2,3-Dichloro-5,6-dicyanobenzoquinone (DDQ)		0.75 <sup>30</sup>	-72.4	Spontaneous ( $\Delta G < 0$ )
Graphene		0.14 <sup>31-32</sup>	-36.7	0
1,1'-dibenzyl-4,4'-bipyridinium dichloride (BV)		-1.12 <sup>18</sup>	+108.1	Not spontaneous ( $\Delta G > 0$ )

potential has a greater tendency to accept electrons. For instance,  $Au^{3+}$  has a larger reduction potential difference than does DDQ from graphene, i.e., more electrons are transferred to  $Au^{3+}$  from graphene than to DDQ. The electrons near the Dirac point of pristine graphene are depleted, and thus the work function of graphene is expected to increase, as shown in Figure 1. Alternatively, 1,1'-dibenzyl-4,4'-bipyridinium dichloride ( $BV^{2+}$ ) has negative reduction potential.<sup>18</sup> In this case, the Gibbs free energy is positive, i.e., the reduction process from  $BV^{2+}$  to  $BV^0$  is not spontaneous and cannot be used to dope graphene. Therefore, instead of using  $BV^{2+}$  directly,  $BV^0$  was prepared using a reducing agent, as described in the experimental section. After  $BV^0$  doping on graphene,  $BV^0$  becomes stabilized by donating electrons to graphene and is thus transformed into  $BV^{2+}$ . As a consequence, the work function is expected to decrease (see Figure 1). The difference in relative reduction potential from graphene determines the amount of electron transfer.

Figure 2a shows sheet carrier density as measured by the van der Pauw method at room temperature. Pristine graphene

synthesized from CVD shows p-doping behavior with a relatively high carrier density of  $1.8 \times 10^{13} \text{ cm}^{-2}$ , which is higher than the previously observed carrier density of  $\sim 10^{12} \text{ cm}^{-2}$ .<sup>8</sup> This may be attributed to oxidation effects that occur when nitric acid is used to remove catalyst film (Ni or Cu). High carrier density may also originate from the effects of multilayer graphene. In this case, the transmittance was 72% at 550 nm, and the corresponding number of layers was roughly 9 (See Supporting Information, S1). Sheet carrier density relies strongly on the number of graphene layers (See Supporting Information, S2).<sup>33</sup> In the case of the monolayer limit, the sheet carrier density approached  $\sim 10^{12} \text{ cm}^{-2}$ , which is in agreement with the results of a previous report. This is expected due to the fact that the sheet carrier density is in principle obtained by multiplying the film thickness to the bulk carrier density.<sup>34</sup> The sheet carrier density (p-type) increased linearly with DDQ and reached  $2.4 \times 10^{13} \text{ cm}^{-2}$  with  $AuCl_3$  doping. The change of the carrier density follows that of the reduction potential.

(31) Trasatti, S. *Pure Appl. Chem.* **1986**, *58*, 955–966.

(32) Reiss, H.; Heller, A. *J. Phys. Chem.* **1985**, *89*, 4207–4213.

(33) Nair, R. R.; Blake, P.; Grigorenko, A. N.; Novoselov, K. S.; Booth, T. J.; Stauber, T.; Peres, N. M. R.; Geim, A. K. *Science*. **2008**, *320*, 1308.

(34) Klein, C. A.; Straub, W. D. *Phys. Rev.* **1961**, *123*, 1581–1583.



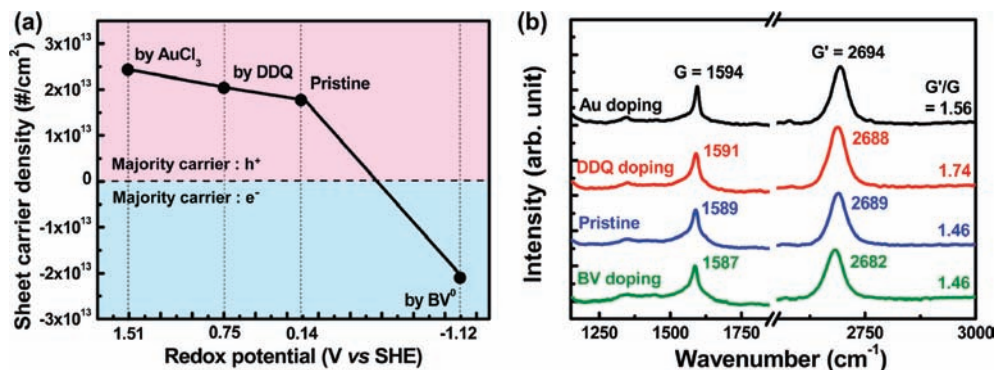


**Figure 2.** (a) Changes of sheet carrier density associated with various dopants. (b) Raman spectra of graphene at 514 nm with various dopants.

**Table 2.** Electrical Properties and Raman Peak Shift of Doped-Graphene Films: Reduction Potentials of Dopant, Sheet Carrier Density, Hall Coefficient, Mobility, Sheet Resistance, and Work Function

dopant	reduction potential (vs SHE) (V)	electrical properties <sup>a</sup>				Raman <sup>b</sup>		
		sheet resistance ( $\Omega/\text{sq}$ )	sheet carrier density ( $\#/\text{cm}^2$ )	mobility ( $\text{cm}^2/\text{V}\cdot\text{s}$ )	work function (eV)	G band shift ( $\text{cm}^{-1}$ )	G' band Shift ( $\text{cm}^{-1}$ )	G'/G ratio
AuCl <sub>3</sub>	1.51	149	$2.4 \times 10^{13}$	1735	4.8	1594	2694	1.56
DDQ	0.75	190	$2.0 \times 10^{13}$	1610	4.7	1591	2688	1.74
pristine GR	0.14	201	$1.8 \times 10^{13}$	1755	4.5	1589	2689	1.46
BV	-1.12	260	$-2.1 \times 10^{13}$	1137	4.0	1587	2682	1.46

<sup>a</sup> Multilayer. <sup>b</sup> Monolayer.

However, in the case of BV doping, the carrier type was converted to n-type and the electron carrier density reached  $2.1 \times 10^{13} \text{ cm}^{-2}$ , which is a similar level to that of AuCl<sub>3</sub> doping. The change of sheet carrier density is strongly related to the difference of the reduction potential, as noted in Table 2. While BV<sup>0</sup> was converted to BV<sup>2+</sup> during doping,<sup>18</sup> some portion of the Au<sup>3+</sup> remained intact.<sup>35</sup> Alternatively, the changes in the mobility were almost negligible for p-dopant, independent of the dopant type in congruent with theoretical prediction,<sup>21</sup> whereas in the case of n-type dopant, the mobility was reduced significantly, in good agreement with potassium doping.<sup>23</sup> It is not clear why mobility was significantly reduced in the case of BV doping. This may be ascribed to the ionic charge scattering of BV<sup>2+</sup> that are present on the graphene surface.<sup>18</sup> This ionic scattering is more dominant than the scattering from Au clusters which is formed by reduction of Au<sup>3+</sup> ions to neutral Au<sup>0</sup>. The conductivity, which is inversely proportional to sheet resistance, is dominated by the sheet carrier density in the case of p-dopant, whereas in the case of n-dopant, the conductivity is dominated by the mobility. The similar doping trend was also observed in the case of monolayer graphene (See Supporting Information, Figure S3a). This implies that the doping can occur for up to  $\sim 10$  graphene layers.

The doping effect was also visible in the G- and G'-band shift and the ratio of G'/G in the Raman spectra, as shown in Figure 2b. The upshift by  $5 \text{ cm}^{-1}$  of Au<sup>3+</sup> doped graphene film with respect to pristine graphene film is evidence of charge transfer from graphene to Au<sup>3+</sup> that enhances electron-phonon coupling, which in turn leads to phonon hardening. The downshift by  $2 \text{ cm}^{-1}$  of BV<sup>0</sup>-treated graphene film indicates charge transfer from BV<sup>0</sup> to graphene, which leads to phonon softening. This concurs with the results of a previous report finding that intentional doping invoked by charge transfer

resulted in a downshift (electron accumulation) and upshift (electron depletion) of the G-band.<sup>36–38</sup> Our result is in good contrast with a simple charge doping without invoking adsorbate adsorption that may create sp<sup>3</sup> hybridization.<sup>39–41</sup> For instance, DDQ involves more  $\pi-\pi$  stacking and therefore sp<sup>3</sup> hybridization or intensity of G' band increased after doping, as shown in Figure 2b. Even for AuCl<sub>3</sub> doping, D-band was increased due to the chemical bonding of Au to the CNT surface.<sup>28,42</sup>

Figure 3 shows the UPS spectra around the secondary-electron threshold region for doped graphene films. The work function  $\Phi$  is determined from the secondary electron energy threshold as  $\Phi = h\nu - E_F + E_{\text{cutoff}}$ , where  $h\nu$ ,  $E_F$ , and  $E_{\text{cutoff}}$  are the photon energy of the excitation light (40.8 eV), the Fermi level edge (42.2 eV in this work), and the measured inelastic high-binding-energy cutoff, respectively.  $E_{\text{cutoff}}$  was determined by using a linear extrapolation of the high binding-energy cutoff region.  $E_{\text{cutoff}}$  of the pristine graphene film was determined to be 5.9 eV, corresponding to a work function of 4.5 eV, which is similar to values drawn from a previous report.<sup>16</sup> Furthermore, the monolayer graphene showed the same work function as multilayer graphene within experimental accuracy (see Supporting Information, Figure S3b). Thus, the reduction potential of graphene is +0.14 V vs a standard hydrogen electrode (SHE).<sup>31,32</sup> This value is much lower than that of Au<sup>3+</sup> (+1.51 V vs SHE). Therefore, the graphene electrons were donated to positively

(36) Rao, A. M.; Eklund, P. C.; Bandow, S.; Thess, A.; Smalley, R. E. *Nature* **1997**, *388*, 257–259.

(37) Nguyen, K. T.; Gaur, A.; Shim, M. *Phys. Rev. Lett.* **2007**, *98*, 145504.

(38) Jishi, R. A.; Dresselhaus, M. S. *Phys. Rev. B* **2007**, *45*, 6914–6918.

(39) Das, A.; Pisana, S.; Chakraborty, B.; Piscanec, S.; Saha, S. K.; Waghmare, U. V.; Novoselov, K. S.; Krishnamurthy, H. R.; Geim, A. K.; Ferrari, A. C.; Sood, A. K. *Nat. Nanotechnol.* **2008**, *3*, 210–215.

(40) Casiraghi, C. *Phys. Rev. B* **2009**, *80*, 233407.

(41) Jung, N.; Kim, N.; Jockusch, S.; Turro, N. J.; Kim, P.; Brus, L. *Nano Lett.* **2009**, *9*, 4133–4137.

(42) Duong, D. L.; Lee, I. H.; Kim, K. K.; Kong, J.; Lee, S. M.; Lee, Y. H. *ACS Nano* **2010**, *4*, 5430–5436.

(35) Benayad, A.; Shin, H.-J.; Park, H. K.; Yoon, S.-M.; Kim, K. K.; Jin, M. H.; Jeong, H.-K.; Lee, J. C.; Choi, J.-Y.; Lee, Y. H. *Chem. Phys. Lett.* **2009**, *475*, 91–95.

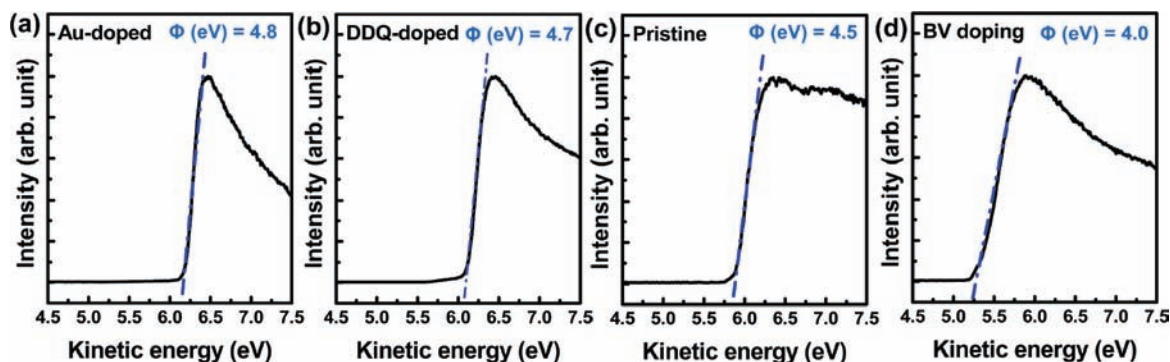


**Figure 3.** UPS spectra around the secondary-electron threshold region for graphenes with different dopants: (a) Au ion, (b) DDQ, (c) pristine graphene, and (d) BV<sup>0</sup>.

charged Au ions. The work functions of Au-doped and DDQ-doped graphene films were increased to 4.8 and 4.6 eV, respectively. However, the work function of the BV-doped graphene film significantly decreased to 4.0 eV. Table 2 summarizes related material doping parameters such as sheet carrier density, mobility, sheet resistance, and related work functions. Sheet resistance was also measured in order to further elucidate the effect of doping on graphene. The sheet resistance of p-doped graphene decreased to 149  $\Omega/\text{sq}$ , compared to 200  $\Omega/\text{sq}$  for pristine graphene film. In the case of BV doping, the sheet resistance increased to 260  $\Omega/\text{sq}$ . Although sheet carrier density increased, mobility decreased. The change of work function with doping was not so prominent but can be clearly distinct from experimental accuracy. This is different from the theoretical prediction that the work function do not alter with doping carrier concentration.<sup>21</sup>

**3.2. Characterization of Nanogenerators by Controlling the Work Function of Graphene Electrodes.** Nanogenerators are composed of two electrodes with a piezoelectric material between them. The electrical energy produced by the generator is harvested by external stimuli such as body movement, vibration, and/or hydraulic forces.<sup>43–45</sup> The placement of a Schottky barrier control between the electrode and semiconducting piezoelectric material is a key method to improve energy harvesting performance.<sup>46–48</sup> We chose ZnO nanorods for use as a semiconducting piezoelectric material in this work. Graphene film was used as the top electrode (see Supporting Information, Figure S4), where the work function of the graphene electrode was maintained within a range of 4.0 to 4.8 eV through the doping approach mentioned previously. Since the electron affinity of ZnO nanorods is usually 4.1  $\approx$  4.35 eV, the Fermi level of n-type ZnO nanorods was chosen as 4.3 eV (average electron affinity of 4.2 eV plus a donor level of 0.1

eV).<sup>49,50</sup> This device has two contacts: ITO/ZnO at the bottom and graphene/ZnO at the top. Since the bottom ITO/ZnO has an ohmic contact,<sup>51</sup> the I–V characteristics are dominated by the nonohmic graphene/ZnO contact.

To examine the effect of the Schottky barrier on nanogenerator performance, we define the work function difference as  $\Delta\Phi = \Phi_{\text{Graphene}} - \Phi_{\text{ZnO}}$ . If  $\Delta\Phi$  is positive and suitably large, then electrons generated from ZnO nanorods by external stimuli will accumulate because of a high Schottky barrier. If  $\Delta\Phi$  is negative, and there is ohmic contact, then the electrons generated in ZnO nanorods will be immediately transported to the graphene electrode. We prepared three different nanogenerators based on different work function-controlled graphene electrodes (pristine, Au-doped graphene and BV-doped graphene). The output currents of these devices were generated by discharging electrons that had accumulated in ZnO nanorods through bending.<sup>43–45</sup>

The effect of the Schottky barrier was demonstrated in I–V characteristics. The off-current in Figure 4a was well quenched in Au-doped graphene film, whereas some leakage current was observed in pristine graphene film due to a shallow Schottky barrier. The on-current level of Au-doped graphene film was larger because of the better sheet resistance of 378  $\Omega/\text{sq}$ , compared to 465  $\Omega/\text{sq}$  for the pristine film. Figure 4b,c shows the output performances of nanogenerators with pristine and Au-doped graphene electrodes. The nanogenerator fabricated with pristine graphene yielded an average current density of 0.2  $\mu\text{A}/\text{cm}^2$  at a load of 0.5 kgf, whereas the nanogenerator fabricated with Au-doped graphene generated a higher average current density of 0.3  $\mu\text{A}/\text{cm}^2$ . The current density of the nanogenerator is altered by the work function difference  $\Delta\Phi$  and the sheet resistance of the electrode. The increase of current density in the Au-doped graphene electrode may be due in part to its relatively low sheet resistance (see on-current levels in Figure 4a). We fabricated two devices using graphene electrodes (pristine and Au-doped) with almost the same sheet resistance by modulating the number of pristine graphene layers in order to isolate the effects of work function difference. As evidenced by the I–V curves in Figure 4d, the on-current levels were similar due to the similar sheet resistances. It is notable that

(43) Wang, X. D.; Song, J. H.; Liu, J.; Wang, Z. L. *Science* **2007**, *316*, 102–105.

(44) Wang, Z. L.; Song, J. H. *Science* **2006**, *312*, 242–246.

(45) Qin, Y.; Wang, X. D.; Wang, Z. L. *Nature* **2008**, *451*, 809–813.

(46) Choi, M.-Y.; Choi, D.; Jin, M.-J.; Kim, I.; Kim, S.-H.; Choi, J.-Y.; Lee, S. Y.; Kim, J. M.; Kim, S.-W. *Adv. Mater.* **2009**, *21*, 2185–2189.

(47) Choi, D.; Choi, M.-Y.; Shin, H.-J.; Yoon, S.-M.; Seo, J.-S.; Choi, J.-Y.; Lee, S. Y.; Kim, J. M.; Kim, S.-W. *J. Phys. Chem. C* **2010**, *114*, 1379–1384.

(48) Choi, D.; Choi, M.-Y.; Choi, W. M.; Shin, H.-J.; Park, H.-K.; Seo, J.-S.; Park, J.; Yoon, S.-M.; Chae, S. J.; Lee, Y. H.; Kim, S.-W.; Choi, J.-Y.; Lee, S. Y.; Kim, J. M. *Adv. Mater.* **2010**, *22*, 2187–2192.

(49) Liu, Y. L.; Liu, Y. C.; Yang, H.; Wang, W. B.; Ma, J. G.; Zhang, J. Y.; Lu, Y. M.; Shen, D. Z.; Fan, X. W. *J. Phys. D: Appl. Phys.* **2003**, *36*, 2705.

(50) Coppa, B. J.; Davis, R. F.; Nemanich, R. J. *Appl. Phys. Lett.* **2003**, *82*, 400–406.

(51) Xu, S.; Qin, Y.; Xu, C.; Wei, Y.; Yang, R.; Wang, Z. L. *Nat. Nanotechnol.* **2010**, *5*, 366–373.

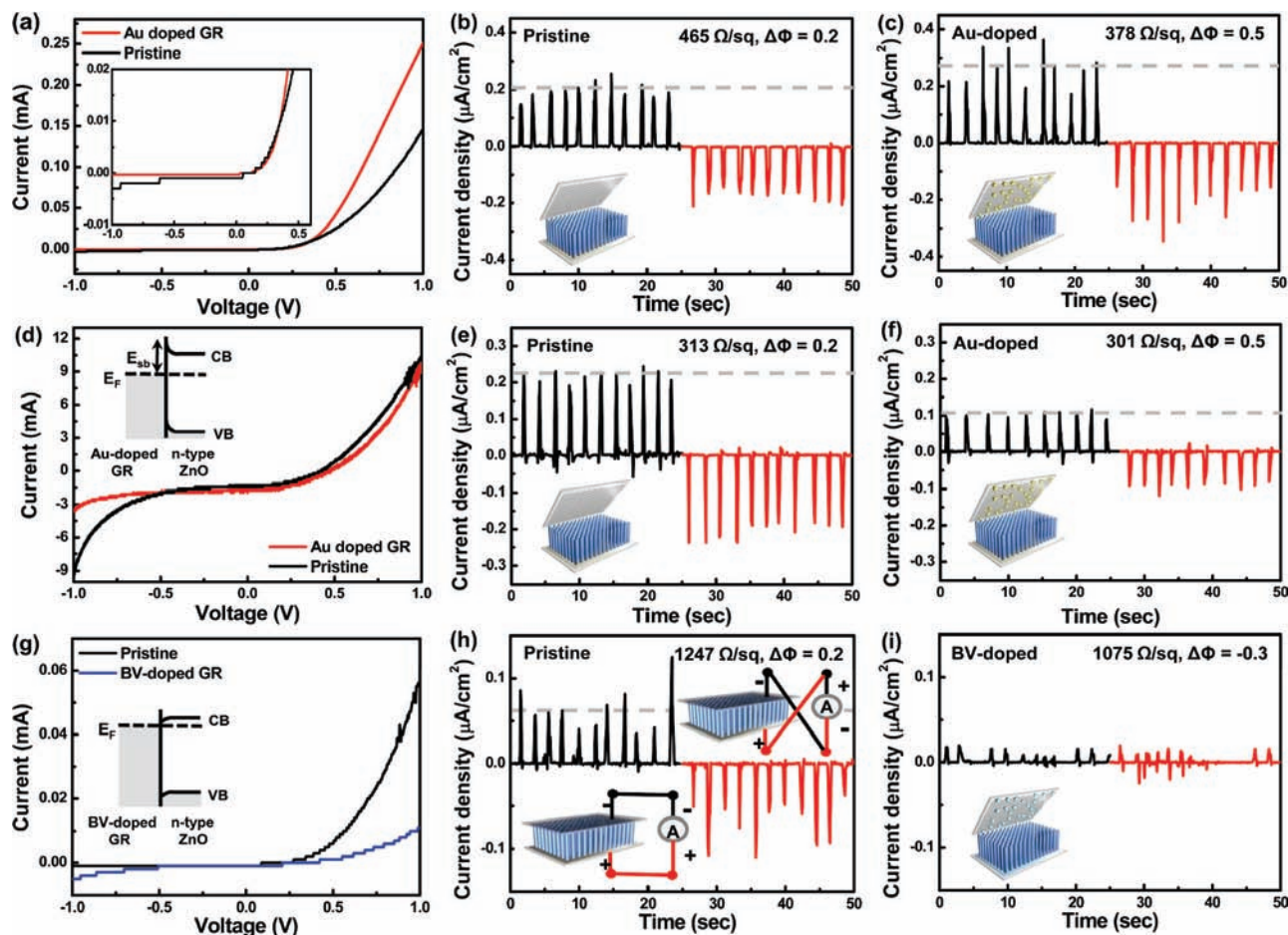


**Figure 4.** I–V curves and output current density of graphene-based nanogenerators with top electrodes made of (a–c) Au-doped graphene with different sheet resistances, (d–f) Au-doped graphene with similar sheet resistances, and (g–i) BV-doped graphene with similar sheet resistances. Doped samples were always compared to pristine samples. The insets of (d) and (g) show band diagrams between the doped-graphene electrode and ZnO nanorod.

the output current level was reduced when the work function difference was large in Au-doped graphene electrodes, although the sheet resistances were similar, as shown in Figure 4e,f. This can be explained by the formation of depletion layer in p–n junction between Au-doped p-type graphene and n-type ZnO nanorods.<sup>52</sup> The p–n junction at the Au-doped graphene–ZnO interface is reversely biased. In this case, the charges are accumulated without releasing due to the rectifying effect of the p–n junction, as shown in Figure 4d.

The current level was significantly reduced due to the negative work function difference, as shown in Figure 4g. Due to the large sheet resistance (1247  $\Omega/\text{sq}$ ) observed in the pristine graphene electrode, relatively small current densities were retained as shown in Figure 4h, but even such small values could be generated owing to the positive work function difference (i.e., Schottky contact). However, in BV-doped film with even smaller sheet resistance (1075  $\Omega/\text{sq}$ ), the current density was negligible due to the negative work function difference (Figure 4i). A positive current pulse is recorded upon compressive strain when the current meter is forward connected to the nanogenerator, and a negative current pulse is recorded when the current meter is reversely connected, a phenomenon known as switching-polarity (Inset of Figure 4h). However, the BV-doped

graphene-based nanogenerator did not exhibit this switching-polarity behavior due to its negative work function difference (Figure 4g). This implies that, although control of the Fermi level is crucial for optimizing the output performance of the nanogenerator, the presence of a hole-doped graphene layer is not beneficial to the performance of a nanogenerator that invokes electron generation. Consequently, not only work function matching, but also the formation of p–n junction at the interface should be taken into account when choosing doped graphene electrodes.

#### 4. Conclusions

We manipulated the electronic structures of graphene using chemical dopants. Work function, sheet carrier density, mobility, and sheet resistance were measured systematically. Dopants were chosen according to the reduction potential value, which was a crucial parameter for determining the electronic properties of graphene.  $\text{AuCl}_3$  (or  $\text{Au}^{3+}$  ion) and DDQ with positive reduction potentials tend to accept electrons. Electrons near the Dirac point of pristine graphene were depleted; thus, the work function of graphene was increased to 4.8 eV, compared to 4.5 eV for pristine graphene. However, BV with negative reduction potential converted the majority carrier type from p-type to n-type, resulting in a decrease in work function to 4.0 eV. The effects of such modulations in work function were demonstrated in a realistic nanogenerator when graphene was used as a top

(52) Song, J.; Wang, X.; Liu, J.; Liu, H.; Li, Y.; Wang, Z. L. *Nano Lett.* 2008, 8, 203–207.



electrode. Not only control of the work function, but also carrier type matching must be taken into account when doped graphene electrodes are used in electrical devices.

**Acknowledgment.** This work was supported by the MOE through the STAR-Faculty Project, TND Project, and World Class University (WCU) Program of KOSEF funded by MEST (R31-2008-000-10029-0), by KICOS through a grant provided by MOST in 2007 (No. 2007-00202), and by KOSEF through CNNC at SKKU.

**Supporting Information Available:** Graphene characterization (Figure S1), the electrical property by layers of graphene (Figure S2), the doping effect of monolayer graphene (Figure S3), and nanogenerator characterization with doped graphene electrode (Figure S4). This material is available free of charge via the Internet at <http://pubs.acs.org>.

JA105140E